



HAL
open science

Chemical mechanisms inducing a dc current measured in the flowing post-discharge of an RF He-O₂ plasma torch

Thierry Dufour, J Hubert, N Vandencastele, F Reniers

► To cite this version:

Thierry Dufour, J Hubert, N Vandencastele, F Reniers. Chemical mechanisms inducing a dc current measured in the flowing post-discharge of an RF He-O₂ plasma torch. *Plasma Sources Science and Technology*, 2012, 21, 045013 (10pp). 10.1088/0963-0252/21/4/045013 . hal-01303168v2

HAL Id: hal-01303168

<https://hal.sorbonne-universite.fr/hal-01303168v2>

Submitted on 15 Jan 2023

HAL is a multi-disciplinary open access archive for the deposit and dissemination of scientific research documents, whether they are published or not. The documents may come from teaching and research institutions in France or abroad, or from public or private research centers.

L'archive ouverte pluridisciplinaire **HAL**, est destinée au dépôt et à la diffusion de documents scientifiques de niveau recherche, publiés ou non, émanant des établissements d'enseignement et de recherche français ou étrangers, des laboratoires publics ou privés.

Title	Chemical mechanisms inducing a DC current measured in the flowing post-discharge of an RF He-O₂ plasma torch
Authors	T Dufour ^{1,2} , J Hubert ¹ , N Vandencastele ¹ and F Reniers ¹
Affiliations	¹ Faculté des Sciences, Service de Chimie Analytique et de chimie des Interfaces, Université Libre de Bruxelles, CP-255, Bld du Triomphe, B-1050 Bruxelles, Belgium ² Sorbonne Université, Campus Pierre et Marie curie, 4 place Jussieu, 75005 Paris, France
Ref.	Plasma Sources Science & Technology, 2012, Vol. 21, Issue 4, 045013 (10 pp)
DOI	http://dx.doi.org/10.1088/0963-0252/21/4/045013
Abstract	The post-discharge of an RF plasma torch supplied with helium and oxygen gases is characterized by mass spectrometry, optical emission spectroscopy and electrical measurements. We have proved the existence of a dc current in the post-discharge (1–20 μA), attributed to the Penning ionization of atmospheric nitrogen and oxygenated species. The mechanisms ruling this dc current are investigated through experiments in which we discuss the influence of the O ₂ flow rate, the He flow rate and the distance separating the plasma torch from a material surface located downstream.

I. Introduction

Atmospheric pressure plasma processes have been actively investigated during the last decades, particularly micro-plasmas, dielectric barrier discharges and plasma torches [1-4]. In a typical plasma torch, the discharge is initiated between two electrodes and expands a directed flow of gas commonly called "jet" or "post-discharge". These plasma sources can be separated into two categories. The first one gathers plasma torches for the generation of thermal plasmas, where the heavy particles and electrons are in thermal equilibrium. They are used for applications including waste remediation, plasma cutting and plasma spraying [5-8]. The second category regroups cold plasma torches in which a non-equilibrium plasma is ignited at atmospheric pressure and at low gas temperatures (typically less than 200°C). The cold plasma torch is always supplied with a carrier gas (usually helium or argon) that can be mixed with a reactive gas (usually oxygen or nitrogen) enabling the generation of a non-thermal flowing post-discharge. In recent years, cold plasma torches have been actively studied as an effective means for biological applications: biofilms, sterilization, decontamination, treatment of living tissues and cells [9, 16-20] but also for surface treatments such as the grafting of nanoparticles on carbon nanotubes, the synthesis of membrane-electrode assembly for fuel cells, etc. [10-15].

Understanding the properties of a treated surface (surface energy, composition, ...) requires a complete understanding of the post-discharge/surface interactions and a background characterization of the mechanisms ruling the flowing post-discharge.

Since a decade, atmospheric He-O₂ plasmas have been extensively studied but only a few articles are focused on the experimental characterization of their flowing post-discharges [21-25]. Simulations predicting their behavior are also quite complicated because of the outstanding number of reactions occurring at atmospheric pressure, because of the interaction of the species (radicals, ions, metastables, dimmers, ...) with the atmospheric air and finally because of turbulences phenomena [26].

In this article, we have characterized a "curtain post-discharge" generated by an RF (27.12 MHz) plasma torch, supplied with helium and oxygen. The design of the plasma source is original in

that the gap between the two flat electrodes is only 1 mm. Moreover its nozzle's section is linear (20 mm by 0.8 mm), thus giving to the post-discharge a curtain geometry. We will first examine the influence of the He-O₂ flow rates on the post-discharge behavior. Despite an RF running mode of the plasma, we will also stress the existence of a DC current (1-20 μA) measured within the post-discharge. The mechanisms governing this DC current are investigated through electrical measurements, mass spectrometry and optical emission spectroscopy. We have also demonstrated how the current measured in the post-discharge can be modified by varying the position of the plasma torch from a fixed substrate.

II. Experimental set-up

II.1. Characteristics of the plasma source

The post-discharge is generated by an RF atmospheric plasma torch from SurfX Technologies (Atomflo™ 400L-Series) [27]. The controller of the plasma source includes an RF generator (27.12 MHz), an auto-tuning matching network and a gas delivery system with two mass-flow controllers to regulate the helium and oxygen gases fueling the plasma torch. The flow rate of helium (carrier gas) and oxygen (reactive gas) can be adjusted from 10 to 20 L/min and from 0 to 0.8 L/min respectively. As presented in figure 1.a, the resulting gas mixture enters through a tube attached to a rectangular housing. Inside, two perforated sheets uniformize the gas flow down the housing. Then, the gas flows around the left and right edges of the upper electrode and passes through a slit in the center of the lower electrode. Plasma is struck and maintained between these electrodes by applying an RF power to the upper electrode while the lower electrode is grounded. The RF power commonly used is comprised between 60W and 160 W. The geometry of the slit is described as "linear" due to the ratio of its aperture length (20 mm) to its width (0.8 mm). For all the experiments performed in this article, the plasma torch was always turned on 20 minutes before any measurement to ensure a steady-state regime and so no thermal effects influences issued from the progressive heating of the plasma torch.

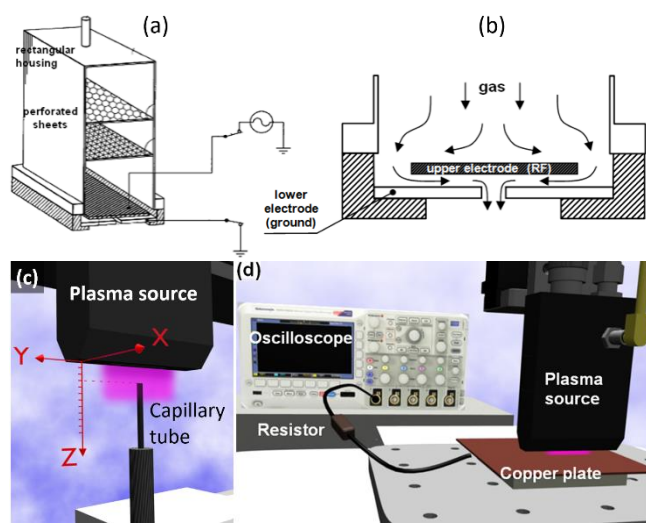


Figure 1. (a) Cross sectional diagram of the RF plasma source (Patent US7329608 SurfX Technologies [Babayan-2008]) (b) Zoom of a (c) Disposition of the capillary tube to the plasma torch for the acquisition of mass spectra (d) Experimental set up to measure DC currents in the flowing post-discharge.

II.2. Diagnostics

Mass spectra of the post-discharge were acquired by a quadrupole mass spectrometer (Balzers QMS 200) coupled with a turbomolecular pump (Pfeiffer TSU 062H) to a base pressure of approximately 1.10^{-8} mbar. The mass spectrometer measured the gaseous species in the post-discharge through a capillary tube, placed in parallel with the gas flow, as illustrated in figure 1.c. The capillary tube is 1m in length, with an inner diameter of 0.01 cm. It is heated by a resistance to maintain the gases temperature at 150 °C, thus avoiding their condensation before entering in the ionization chamber. The ionization energy was set to 70 eV, as it is usually found in the literature [28, 29].

Optical emission spectroscopy was performed with the SpectraPro-2500i spectrometer from ACTON research Corporation (0.500 m focal length, triple grating imaging). Light emitted by the post-discharge was collected by an optical fiber and transmitted to the entrance slit (50 μm) of the monochromator. There, the light is collimated, diffracted, focused on the exit slit and finally captured by a CCD camera from Princeton Instruments. Each optical emission spectrum was acquired with the 1800 grooves. mm^{-1} grating (blazed at 500 nm) and recorded on 30 accumulations with an exposure time of 25 ms. Experimentally, we observed that an increase in the O_2 flow rate was always inducing a decrease in all the emission lines/bands of the post-discharge. As a consequence, from an oxygen flow rate to another one, the deexcitation of a specific species was always proportional to the overall decay of the post-discharge emission. To solve this problem, for every O_2 flow rate, the emissions of all the species were divided by the emission of the whole post-discharge (i.e. a continuum ranging from 250 nm to 850 nm).

Line-absorption spectroscopy was applied to evidence He (2^3S) metastable states, more precisely on the transition $2^3\text{S}-3^3\text{P}$ at

388.9nm. This method was reliable and only required an external light source emitting the appropriate wavelength. The absorption rate A is related to the emission intensities by the relation $A=(I_L+I_p-I_{L+p})/I_L$, where I_p is the light intensity emitted from the post-discharge, I_L is the line intensity from the external lamp and I_{L+p} is the line intensity from the two light sources [30, 31]. The light intensities were measured by placing the optical fiber along the Y-axis (see figure 1.c), 1cm away from the post-discharge.

To measure a DC current in the post-discharge, we introduced a copper plate downstream, as illustrated in figure 1.d. We called "gap" the distance separating the plasma source's top head from the copper plate. The current was obtained by measuring the potential difference across a resistor (820 $\text{k}\Omega$) connecting the copper plate to an oscilloscope. For an accurate representation of the signals, we used a digital phosphor oscilloscope from Tektronix (DPO 3032) with a bandgap of 300 MHz and a sample rate as high as 2,5 GS/s.

III. Results and discussion

In this section, we discuss how the current measured in the flowing post-discharge is depending on the O_2 flow rate, the helium flow rate and on the gap (distance separating the plasma source from a substrate placed downstream). The measurement of a DC current in the post-discharge is correlated with chemical reactions evidenced by means of mass spectrometry, optical emission/absorption spectroscopy.

III.1. Influence of the O_2 flow rate

III.1.1. Results from MS

The mass spectra of the air (grey curve) and of the flowing post-discharge supplied in helium gas (black curve) are represented in figure 2. The mass spectrum of the air shows m/z ratios at 14, 16, 28 and 32 corresponding to the N, O, N_2 and O_2 species respectively. N_2 and O_2 are basic compounds of the air which is not the case for atomic O and N. Actually, the peaks at 14 and 16 represent N^+ and O^+ species (and/or doubly charged molecular ions N_2^{2+} and O_2^{2+}) produced in the ionization chamber of the mass spectrometer. The high electron energy (70 eV) allows the fragmentation of the O_2 and N_2 molecules by dissociative ionization processes. Peaks measured at 14 and 16 represent a background (intrinsic to the ionization chamber). The same remark applies for the peak at $m/z = 30$ indicating the production of nitric oxide molecules (NO) in the ionization chamber as a product of atomic O and N. The mass spectrum of the post-discharge (black curve in figure 2) is obtained for a distance of 1 mm separating the capillary tube from the plasma torch. This mass spectrum shows that the amounts of N_2 and O_2 become lower and the products of their reactions ($m/z = 14, 16, 30$) as well. Moreover the argon peak ($m/z = 40$) disappears while the CO_2 peak ($m/z = 44$) is reduced in size. Of course, a very elevated peak of helium is measured at $m/z = 4$.

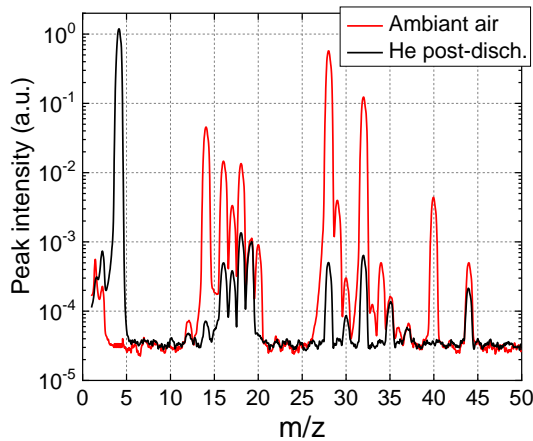


Figure 2. Mass spectrum of the atmospheric air (grey curve) and mass spectrum of the flowing post-discharge (black curve) only supplied in helium gas, with $\Phi(\text{He}) = 15 \text{ L/min}$, $P_{\text{RF}} = 120\text{W}$ and $Z_{\text{capillary}} = 1 \text{ mm}$.

Now that we have evidenced the fragmentation phenomenon of molecules in the ionization chamber, a flowing post-discharge only supplied with $\Phi(\text{He}) = 15 \text{ L/min}$ (figure 3.a) is compared to a flowing post-discharge supplied with $\Phi(\text{He}) = 15 \text{ L/min}$ and $\Phi(\text{O}_2) = 300 \text{ mL/min}$ (figure 3.b). For these two cases, the peaks of helium, nitrogen and oxygenated species have been spatially measured by positioning the capillary tube at different positions along the Z-axis of the plasma source, as indicated in figure 1.c.

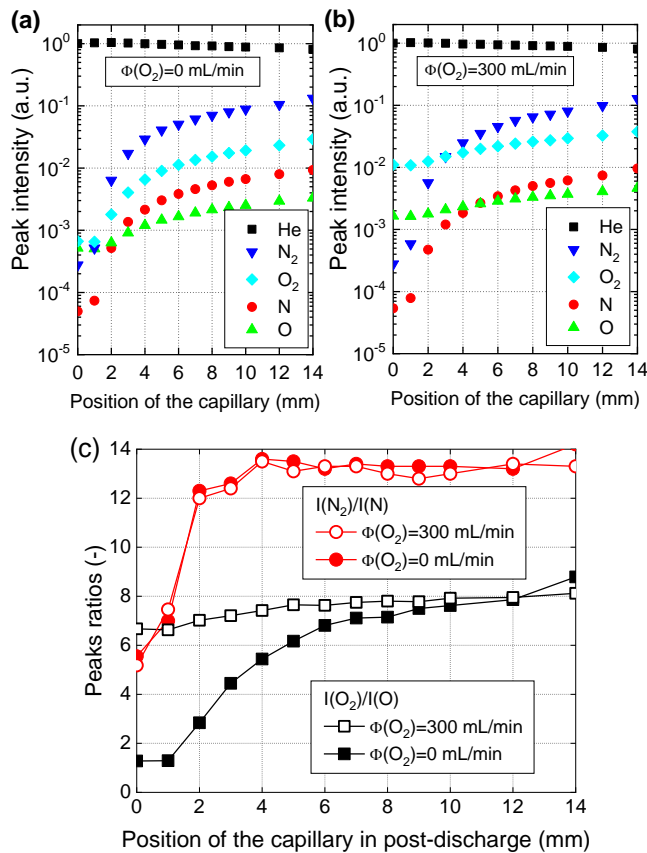


Figure 3. Spatial resolution along the Z-axis of the He, N, N_2 , O and O_2 peaks intensities for $\Phi(\text{He}) = 15 \text{ L/min}$, $P_{\text{RF}} = 120\text{W}$ and (a) $\Phi(\text{O}_2) = 0$

mL/min (b) $\Phi(\text{O}_2) = 300 \text{ mL/min}$. (c) Peaks ratios of nitrogen species and oxygen species.

In figure 3.a, the chemical composition of the post-discharge is not homogeneous along the Z-axis. For a position of the capillary tube higher than $Z=2 \text{ mm}$, the nitrogen and oxygenated species are no more negligible and represent potential sources of contamination in the treatment of surfaces [32]. In figure 3.b, the injection of O_2 at 300 mL/min is detected in the post-discharge and the production of O as well. The O-profile along the Z-axis is more elevated in figure 3.b than in figure 3.a. due to the dissociation of the injected O_2 . Two sources of atomic oxygen must be considered: the fragmentation of the atmospheric O_2 in the ionization chamber (which applies in both cases) and the plasma source (which only applies in the second case). However, the two atomic nitrogen profiles show no difference thus indicating that they are only produced in the ionization chamber of the mass spectrometer.

As those nitrogen and oxygenated species exist in the flowing post-discharge, they represent a potential source of contamination in the treatment of surfaces. We compared this contamination (nitrogen and oxygenated species) to the contamination measured in a usual low-pressure plasma chamber, i.e. a Pyrex bell jar, only filled by atmospheric air and connected to a primary pumping. The pressure in this vacuum chamber was controlled by a Baratron gauge for a set of pressures ranging from 1 Torr to 760 Torr. As illustrated in figure 4, the peaks intensities of the nitrogen and oxygenated species have been plotted versus the pressure in the case of the RF plasma torch (open symbols) and in the case of the vacuum chamber (filled symbols). This figure shows that the contamination in our atmospheric post-discharge (for $Z < 2 \text{ mm}$) is similar to the contamination in a vacuum chamber working under a pressure of about 1 Torr. The surface contamination induced by the flowing post-discharge during the process is controlled over time, potentially negligible on the treatment of surfaces, but not necessarily negligible on the plasma chemistry as we will discuss now through OES and OAS experiments.

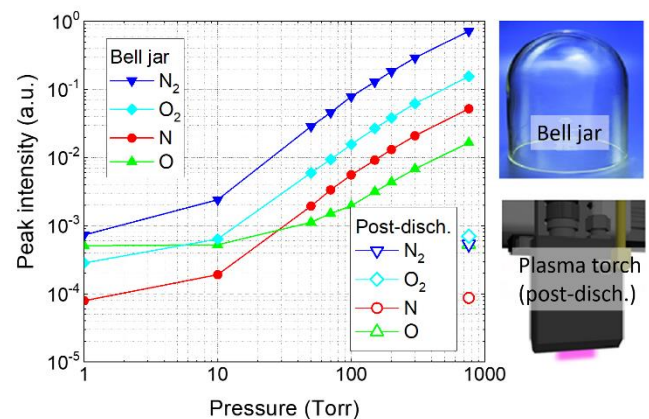


Figure 4. Peaks intensities of nitrogen and oxygenated species versus the pressure for two cases: the RF plasma torch (operating only at 760 Torr for $\Phi(\text{He}) = 15 \text{ L/min}$, $\Phi(\text{O}_2) = 0 \text{ mL/min}$, $P_{\text{RF}} = 120\text{W}$ and $Z_{\text{capillary}} = 1 \text{ mm}$) and a usual vacuum chamber.

III.1.2. Results from OES and OAS

In figures 5.a and 5.b, the emission intensities of several species are plotted versus the O₂ flow rate: N₂ (337 nm), N₂⁺ (391 nm), He (3³S, 706.5 nm), O (3³S, 844.6 nm), OH (310 nm), O₂(b¹Σ_g⁺, 765 nm) and O₂⁺ (525 nm). Production of O, O₂⁺ and O₂(b¹Σ_g⁺) species (increasing curves) is balanced by the consumption of He, OH, N₂ and N₂⁺ (decreasing curves). We have also reported in figure 6 the emission spectra of O₂(b¹Σ_g⁺), N₂⁺ and O₂⁺ as they are rarely presented in the literature when measured in a post-discharge. The band of the singlet sigma metastable oxygen O₂(b¹Σ_g⁺) was measured between 758 nm and 770 nm; it lies closely above the O₂(a¹Δ_g) excited singlet state and O₂(X³Σ_g⁻) triplet ground state [33-35]. To evidence the 2³S metastable states of helium, we have reported in figure 7 its absorption rate versus the O₂ flow rate obtained by line-absorption spectroscopy on the transition He(3³P-2³S) at 388.9nm. All those results will be now discussed for each species to draw up the main chemical mechanisms in the flowing post-discharge.

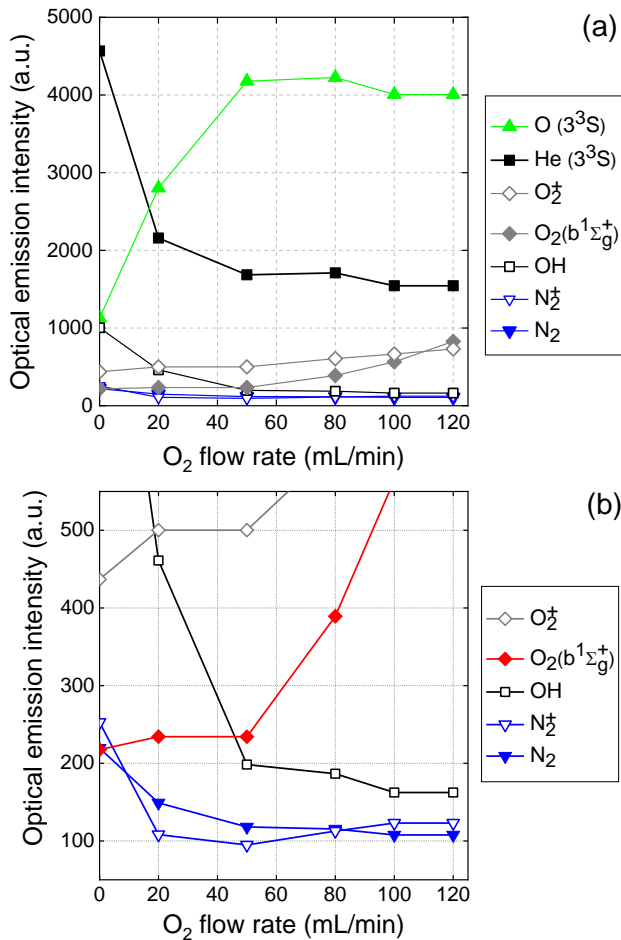


Figure 5. (a) Optical emission spectra of the whole post-discharge versus the O₂ flow rate for $\Phi(\text{He}) = 15 \text{ L/min}$, $P_{\text{RF}} = 120\text{W}$ and $\text{gap} = 5 \text{ mm}$. (b) Zoom of figure 5.a.

O₂⁺ ions

From 0 to 120 mL/min, the increase in the O₂ flow rate is accompanied by a permanent increase in O₂⁺ ions, as illustrated in

figure 5.b. Several mechanisms are usually considered to explain the production of O₂⁺ but all cannot apply here. Thus, a charge transfer reaction involving O₂ molecules and O⁺ ions is not possible since no emission of O⁺ was detected at 465 nm [36]. A dissociative charge transfer with He₂⁺ ions is not possible either since no emission intensity was detected from the He₂ band (3pπe³Π_g-2sσa³Σ_u⁺) between 462 nm and 468 nm [37]. The electron impact ionization of O₂ (Reaction [A] in Table 1) is possible but seems negligible due to the low value of its rate constant and also because of the usual weak electron densities measured in similar He-O₂ RF post-discharges (between 8.10¹⁰ cm⁻³ and 1.3.10¹² cm⁻³ [13]). The main mechanism explaining the production of O₂⁺ ions is the Penning ionization of O₂ molecules by He metastables (Reaction [B] in Table 1). Such a reaction requires He (2³S) metastables that will be evidenced afterwards, and produces – in addition to O₂⁺ ions – electrons and radiative states of helium.

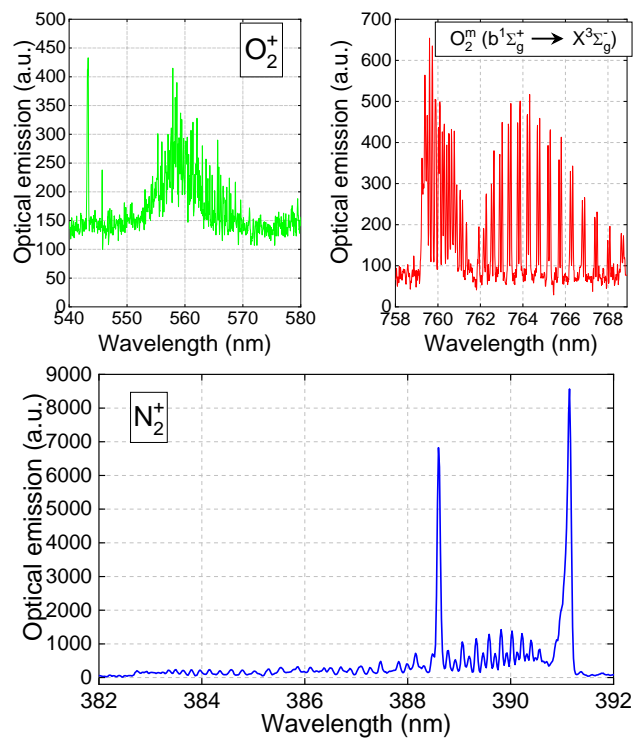


Figure 6. Optical emission spectra of O₂ metastables, O₂⁺ ions and N₂⁺ ions measured in the flowing post-discharge for the following experimental conditions (a & b) $\Phi(\text{He}) = 15 \text{ L/min}$, $\Phi(\text{O}_2) = 100 \text{ mL/min}$, $P_{\text{RF}} = 120\text{W}$, $\text{gap} = 6 \text{ mm}$, (c) $\Phi(\text{He}) = 15 \text{ L/min}$, $\Phi(\text{O}_2) = 0 \text{ mL/min}$, $P_{\text{RF}} = 120\text{W}$, $\text{gap} = 5 \text{ mm}$.

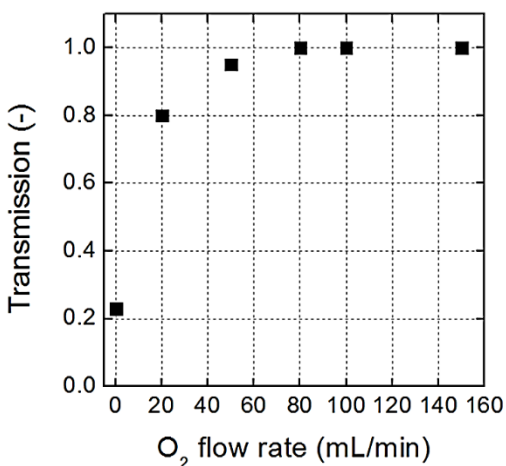


Figure 7. Transmission of He 2^3S at 388.9 nm, in the He- O_2 flowing post-discharge with $\Phi(\text{He}) = 15 \text{ L/min}$, $\Phi(O_2) = 0 \text{ \& } 100 \text{ mL/min}$ and $P_{RF} = 120 \text{ W}$.

N_2^+ ions

At atmospheric pressure, the production of N_2^+ ions could be attributed to three known mechanisms: a charge transfer from He_2^+ ions to N_2 , a charge transfer from He^+ ions to N_2 and the Penning ionization of N_2 from metastable helium (Reaction [C]). As we did not detect any emission intensity from He_2 and He^+ species in our experiments, the reaction [C] is considered as the main source of $N_2^+(B^2\Sigma_u^+)$ ions. This last reaction has been widely studied in low-pressure experiments [38-41] and is considered at atmospheric pressure as the major mechanism to produce $N_2^+(B^2\Sigma_u^+)$ ions [24]. We also observed the emission of $N_2^+(X^2\Sigma_g^+)$ species on the (0-0) band of the first negative system at 391.4 nm (Reaction [D]). The figure 5.b also indicates in which extent the O_2 species influence the Penning ionization of $N_2(X^1\Sigma_g^+)$. Thus, a flow as low as 20 mL/min in O_2 reduces by more than 50% the emission of $N_2^+(B^2\Sigma_u^+)$. The explanation to this decrease can be found in the absorption peak of He (2^3S) represented in figure 7. The absorption rate is drastically reduced by increasing the O_2 flow rate. He (2^3S) metastables are consumed as mentioned in the reaction [B], thus becoming a limiting reactant in reaction [C]. As the reaction [C] becomes less preponderant, the emission of $N_2^+(B^2\Sigma_u^+)$ decreases with the increase in the O_2 flow rate.

Atomic oxygen

For $\Phi(O_2)=0-50 \text{ mL/min}$, the increase in the O (3^3S) emission is consistent with our previous results from mass spectrometry (figures 3.a and 3.b) in which atomic oxygen was only produced when O_2 was injected in the discharge. The direct dissociation of O_2 molecules through collisions with energetic electrons is obviously inefficient, because of the electronegative nature of O_2 [42]. The most probable channel to produce atomic oxygen is the Penning ionization of O_2 molecules (Reaction [B]) followed by the electron impact dissociation of O_2^+ (Reaction [E]). The rate constant of this last reaction ($4.8 \cdot 10^{-7} \text{ cm}^3 \cdot \text{mol}^{-1} \cdot \text{s}^{-1}$) is particularly elevated. For $\Phi(O_2) = 50-120 \text{ mL/min}$, the emission intensity of O (3^3S) has reached a plateau that can be interpreted as resulting from an equilibrium between production and consumption mechanisms.

Helium species

The Grotrian diagrams of He I and O I indicate that radiative states of helium present energetic levels almost twice higher than those of oxygen [43]. It is suspected that the addition of 1% of an electronegative gas, namely O_2 , in the inert helium gas causes a reduction of the electron density so that the electron collisional processes can no longer participate to the excitation of the He radiative states [44]. In figure 5.a, for O_2 flow rates increasing from 0 mL/min to 50 mL/min, we have registered a decay in the emission of He (3^3S) counterbalanced by the production of radiative O (3^3S) at 844.6 nm. The same emission decay from He radiative states was measured by increasing the O_2 flow rate of an atmospheric plasma jet sustained by helium [36]. Moreover, another experiment performed in a He- O_2 microwave discharge at atmospheric pressure, indicates a decrease in the density of He (2^3S) metastable states as a function of the oxygen concentration in helium, thus following – according to the authors – a similar emission intensity trend as the excited He atoms at 706 nm [23]. Now, for O_2 flow rates increasing from 50 mL/min to 120 mL/min, the emission intensity of the He (3^3S) remains almost constant which is also consistent with the plateau of the O (3^3S) species.

O_2 metastable molecules

For $\Phi(O_2)=0-50 \text{ mL/min}$, the reactions [B] and [F] apply so that all the injected O_2 molecules are both Penning-ionized to produce O_2^+ ions and excited by electrons to produce $O_2(b^1\Sigma_g^+)$ species. According to their respective rate constants, the production of O_2^+ ions is more efficient than the production of $O_2(b^1\Sigma_g^+)$ metastables, which is consistent with their optical emissions intensities: for $\Phi(O_2)$ increasing from 0 to 50 mL/min, the emission of O_2^+ is always higher than the emission of $O_2(b^1\Sigma_g^+)$. Beyond 50 mL/min, the drastic increase in the emission of $O_2(b^1\Sigma_g^+)$ let us think that another channel for the production of $O_2(b^1\Sigma_g^+)$ is opened. The O_2 molecules that were all consumed by the reactions [B] and [F] are from now on in excess, colliding with O (1D) atoms to produce atomic oxygen and $O_2(b^1\Sigma_g^+)$ species, as reported in the reaction [G]. $O_2(a^1\Delta_g)$, which is another metastable state of oxygen, is known to have a lifetime much more longer than $O_2(b^1\Sigma_g^+)$ [45]. The corresponding transition $2a^1\Delta_g \rightarrow 2X^3\Sigma_g^-$ is commonly measured at 1.27 μm by infrared emission spectroscopy or in the visible range at 634 nm and 703 nm by OES [46]. Despite its very long lifetime, no emission intensity of $O_2(a^1\Delta_g)$ was detected in the flowing post-discharge, neither at 634 nm, nor at 703 nm. The absence of this metastable radiative decay can be explained by the existence of other processes which consume more efficiently the $O_2(a^1\Delta_g)$: either by quenching with O_2 molecules (Reaction [H]), and/or to a lesser extent by electronic dissociative attachment (Reaction [I])

OH molecules

At atmospheric pressure, hydroxyl radicals (OH) are mainly produced by electron-impact dissociation of H_2O molecules (single step process) or by electron-impact ionization of H_2O followed by dissociation of H_2O^+ to produce OH (two-step process) [26, 53, 54]. As those reactions require energetic electrons (higher than 2 eV), they probably do not occur in the flowing post-discharge [13, 55]. The production of the OH radicals is assumed to be performed

between the electrodes, where H₂O molecules are adsorbed when the plasma torch is not operating. Moreover, the injection of O₂ in the post-discharge is assumed to decrease the electron density, thus limiting the production of hydroxyl radicals and therefore their emission intensity. For this reason, a decrease in the OH emission is observed in figure 5.a for increasing O₂ flow rates.

	Reaction	Rate constant (cm ³ .mol ⁻¹ .s ⁻¹)	Ref.
A	O ₂ + e → 2e + O ₂ ⁺	3.3.10 ⁻¹⁵	[47]
B	He(2 ³ S) + O ₂ → He + O ₂ ⁺ + e	2.4.10 ⁻¹⁰	[48]
C	He(2 ³ S) + N ₂ (X ¹ Σ _g ⁺ , v = 0) → He + N ₂ ⁺ (B ² Σ _u ⁺ , v' = 0) + e	6.9.10 ⁻¹¹	[36]
D	N ₂ ⁺ (B ² Σ _u ⁺ , v' = 0) → N ₂ ⁺ (X ² Σ _g ⁺ , v = 0) + hν	-	[49]
E	O ₂ ⁺ + e → 2O	4.8.10 ⁻⁷	[48]
F	O ₂ + e → O ₂ (b ¹ Σ _g ⁺) + e	3.1.10 ⁻²⁶	[21]
G	O(1D) + O ₂ → O + O ₂ (b ¹ Σ _g ⁺)	3.08.10 ⁻¹¹	[50]
H	O ₂ (a ¹ Δ _g) + O ₂ → O ₃ + O	2.9.10 ⁻²¹	[51]
I	O ₂ (a ¹ Δ _g) + e → O ⁻ + O	2.3.10 ⁻²²	[52]
J	O ₂ + O ⁺ → O ₂ ⁺ + O	2.0.10 ⁻¹⁰	[47]
K	N ₂ + O → NO + N	3.9.10 ⁻²²	[44]

Table 1. Partial list of reactions with their rate constants for the He-O₂ flowing post-discharge.

Species that have not been observed

In agreement with our previous results from mass spectrometry, no optical emission intensity from atomic nitrogen could be observed at 575 nm or 746 nm. No emission from O⁺ ions could be observed a 465 nm because either they do not exist, or they are quenched by O₂ molecules according to the reaction [J]. The emission intensities from the Rydberg-Rydberg transitions of the NO molecule have not been observed either [56], since the only mechanism allowing its formation is the reaction [K] requiring a gas temperature higher than 1400 K. This temperature is quite higher than the one we measured in the post-discharge (almost 400 K), obtained by fitting the experimental OH band (310 nm) to the OH model computed on the LIFBASE software. The study of the ozone (O₃) concentration by optical absorption spectroscopy has not been carried out due to the small size of the post-discharge. It could participate to the production of other species but it is not directly suspected to sustain the DC current measured in the flowing post-discharge.

Those OES results have highlighted the existence of excited and positive charged species in the flowing post-discharge and suggested mechanisms explaining their production and consumption rates. Two separate Penning ionizations have been highlighted as the major mechanisms allowing the productions of N₂⁺ and O₂⁺ species. According to their rate coefficients, the Penning ionization induced by O₂ (k = 2.4.10⁻¹⁰ cm³.mol⁻¹.s⁻¹) is faster than the Penning ionization induced by N₂ (k = 6.9.10⁻¹¹ cm³.mol⁻¹.s⁻¹). For this reason, the Penning ionization with O₂ molecules quenches the majority of He metastable atoms. As a consequence, very few of them remain available for the Penning ionization of the N₂ molecules, thus explaining why in figure 5.a the emission intensity of N₂⁺ is lower than the emission intensity of O₂⁺.

III.1.3. Electrical measurements

a) Evidence of a DC current measured in the post-discharge

We have evidenced the production of positive charged species (O₂⁺, N₂⁺) which, combined to the gas flow sustained by the plasma torch, could generate an electrical current. To evidence this current, a copper plate was placed 1 mm downstream from the plasma torch to collect the charged species carried away by the flowing post-discharge (see figure 1.d). Then, the resulting current was measured across a resistor connecting the copper plate to the oscilloscope.

The variation of the post-discharge current versus time is plotted in figure 8 for several O₂ flow rates at Φ(He)=15 L/min and an RF power of 120W. The main feature of these currents is the absence of any RF frequency or even AC component. All are pure DC currents, induced by a convective transport of charged species within the flowing post-discharge. The instant t=0 min corresponds to the injection of a O₂ flow rate. Initially, the current measured for Φ(O₂)=100 mL/min is 4 μA and increases drastically to 21 μA within only a few seconds. Then, it decreases over 4 min by following a first-order exponential decay to finally reach the value of 12 μA. These two characteristic times are conditioned by the transport time of O₂ in the gas line and the response time of the mass flow controllers integrated to the plasma source device. Also, these characteristic times do not depend significantly on the O₂ flow rates as their orders of magnitudes are the same whatever the O₂ flow rates (50, 100 or 150 mL/min). In any case, the steep increase subsequently followed by the slow decay constitute a transition regime of approximately 4 minutes. A lower O₂ flow rate does not involve a longer transit time in the gas tubing and therefore not a longer exponential decay as illustrated in the figure 8. As the permanent regime is considered to start at 4 min, all the currents plotted in this article were only measured at least 5 minutes after the injection of O₂ to be sure of their reproducibility.

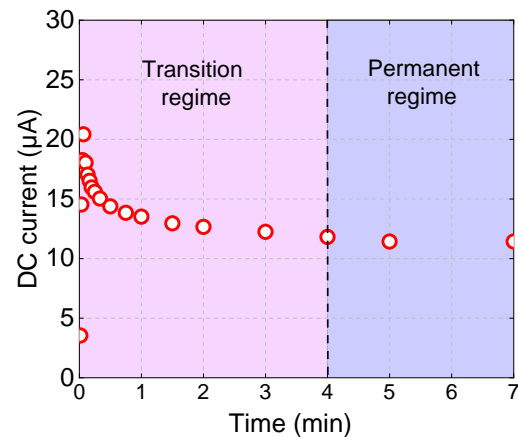


Figure 8. Evolution of the post-discharge DC current versus time, for Φ(He) = 15 L/min, Φ(O₂) = 100 mL/min, P_{RF} = 120W and gap = 1 mm. The O₂ gas was injected at t = 0 min.

b) Experimental study of the permanent regime

The effect of the O₂ gas on the DC current has been investigated for flow rates ranging from 0 to 150 mL/min with a helium flow rate fixed at 15 L/min and an RF power at 120W. The figure 9

shows two operating regimes: for O_2 flow rates increasing from 0 to 50 mL/min, the DC current increases from 3 to 20.5 μA and for O_2 flow rates increasing from 50 to 150 mL/min, it decreases from 20.5 to 3 μA . During the first operating regime, the Penning ionization induced by O_2 (Reaction [B]) becomes always more efficient until a critical flow rate fixed at $\Phi(O_2)=50$ mL/min and for which a maximum current is reached (20.5 μA). Just for recall, this critical flow rate was previously mentioned concerning the OES results in figure 5.a, especially because it was marking the end of the O_2 metastables plateau and the beginning of the atomic oxygen plateau.

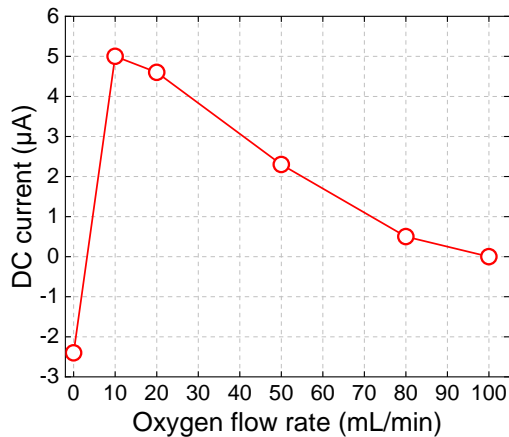


Figure 9. Variations of the DC current measured in the steady flowing post-discharge, versus the O_2 flow rate for $\Phi(He) = 15$ L/min, $P_{RF} = 120W$ and gap = 1 mm.

Beyond this threshold (50 mL/min), the current decreases while according to the emission intensities in figure 5.b: (i) the production of O_2^+ ions increases and (ii) the production of atomic oxygen is leveled on a plateau. A mechanism that could explain the decrease in the current is a rate competition between the permanent production of O_2^+ ions and the production of negative charged species (such as O^- , O_2^-). The production of oxygen negative ions seems a consistent assumption because species with high electronegativity such as O tend to form electronegative ions by the recombination of electrons and radicals at low energies [57]. Moreover, charge neutralization between N_2^+ , O_2^+ and oxygen negative ions may be elevated due to the atmospheric pressure. By increasing the O_2 flow rate, the charge neutralization in the plasma could become more efficient, thus decreasing the plasma density and therefore reducing the post-discharge current. The current measured on the copper plate would be the sum of a positive and a negative component counteracting once the threshold of 50 mL/min is reached.

Another reason that could explain the decrease in the DC current would be the observed reduction in size of the flowing post-discharge when the O_2 flow rate is increased. As the gap remains constant, reducing in size the post-discharge means a less efficient collection of charged species on the copper plate.

III.2. Influence of the He flow rate

III.2.1. Results from OES

The influence of the helium flow rate on the properties of the flowing post-discharge have been investigated by OES. In figure 10, the emission intensities of the previous species are plotted versus the helium flow rate for values ranging from 10 to 20 L/min. The O_2 flow rate is fixed at 100 mL/min and the RF power still at 120 W. The only increasing curve corresponds to the emission of the atomic oxygen at 777 nm. It represents a more significant convective transport of the atomic oxygen along the flow axis of the post-discharge. This phenomenon has already been observed in the case of a He- O_2 plasma-jet [36] and can be explained by the difference of energy between the upper energy level of the O (777 nm) and the upper energy level of He (706 nm): 10.74 eV and 22.72 eV, respectively.

All the other emission intensities slightly decrease versus $\Phi(He)$. The slight decrease in the emission of N_2^+ ions is attributed to the fact that by increasing the helium flow rate, the post-discharge grows bigger, and the nitrogen contamination decays. Therefore, the $N_2(X^1\Sigma_g^+)$ species involved in the Penning ionization (Reaction [C]) limit this reaction, and a slight decrease in the emission of the N_2^+ ions is then observed. The slight decay in the emission of the O_2^+ ions operates on the same principle: the growing post-discharge slightly reduces the atmospheric O_2 component that could participate in the Penning ionization (Reaction [B]).

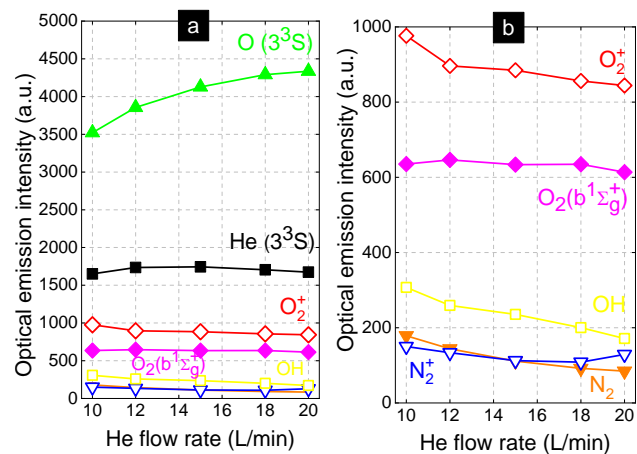


Figure 10. (a) Optical emissions of O, He, O_2^+ , O_2^* , OH, N_2 and N_2^+ versus the helium flow rate for $\Phi(O_2) = 100$ mL/min, $P_{RF} = 120$ W and gap = 5 mm. (b) Zoom of "(a)".

III.2.2. Electrical measurements

In figure 11, for a O_2 flow rate as high as 100 mL/min injected in the flowing post-discharge, the DC current measured for $\Phi(He)=10$ -20 L/min, slightly decreases from 19 μA to 16.5 μA . This behavior is consistent with the emission intensities of the N_2^+ and O_2^+ ions, also slightly decreasing in figure 10. The same behavior is also obtained without supplying the post-discharge in oxygen gas; the resulting DC current is again slightly decreasing but for values approximately 4 times lower than in the previous case.

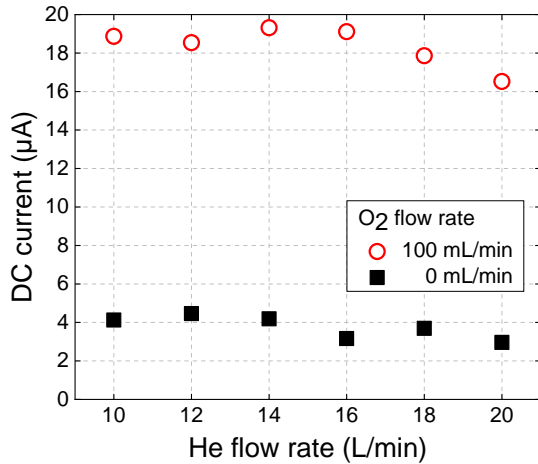


Figure 11. Variations of the DC current in the steady flowing post-discharge versus the helium flow rate for $P_{RF} = 120\text{ W}$ and $\text{gap} = 1\text{ mm}$.

III.3. Influence of the torch/substrate distance: electrical measurements

The interaction of the flowing post-discharge with a surface (the copper plate) has been investigated through electrical measurements. As illustrated in figure 12, the DC current has been measured for different gaps ranging from 1 to 15 mm in two cases: with a O_2 flow rate of 100 mL/min (open symbols) and without injection of O_2 in the post-discharge (filled symbols).

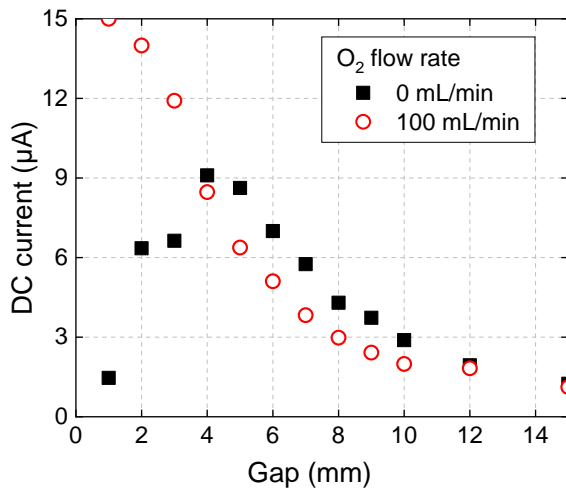


Figure 12. Variations of the DC current versus the gap (distance torch-surface) for $\Phi(\text{He}) = 15\text{ L/min}$, $P_{RF} = 120\text{ W}$ and $\Phi(\text{O}_2) = 0\text{-}100\text{ mL/min}$.

For $\Phi(\text{O}_2) = 100\text{ mL}\cdot\text{min}^{-1}$, the DC current which is about 15 μA for a gap of 1 mm drops to a value less than 1 μA for gaps higher than 14 mm. By increasing the gap, the copper plate collects less positive charged species (N_2^+ and O_2^+ ions), thus inducing an exponential decay of the DC current. It is also worth mentioning that whatever is the gap, the DC current remains always positive: the positive charged species have therefore a lifetime assumed to be longer than the one of the potential oxygenated negative charged species.

For $\Phi(\text{O}_2) = 0\text{ mL}\cdot\text{min}^{-1}$, the increase in the gap is not only reflected by a monotone decrease in the DC current. Such a decrease (filled symbols) is only confirmed for gaps comprised between 4 and 15 mm. On this range, this decrease overlays the previous current decay (open symbols) for the same reasons. However, for gaps comprised between 1 and 4 mm, the current clearly increases from 1 μA (at 1 mm) to 9 μA (at 4 mm). This trend could be explained by two mechanisms: either a more efficient production of positive charged species or a more efficient consumption of oxygenated negative charged species. As no O_2 is injected in the plasma torch, this second assumption seems irrelevant. Therefore, we consider a stronger production of positive charged species which corresponds to the production of N_2^+ by Penning ionization of N_2 . As previously shown by the OES measurements, this reaction ([C]) cannot occur for $\Phi(\text{O}_2) = 100\text{ mL}\cdot\text{min}^{-1}$ as the Penning ionization of O_2 consumes more rapidly the helium metastable species that are necessary to produce N_2^+ . The figure 13 illustrates the two cases (with/without oxygen) and shows the regions where the Penning ionizations are assumed to occur according to the current measurements. This figure illustrates that the Penning ionization of N_2 is maximal if no oxygen is injected in the post-discharge and for a gap of 4 mm. There, the turbulent regime of the flowing post-discharge allows an optimal convective mixture with the atmospheric species, in particular with N_2 .

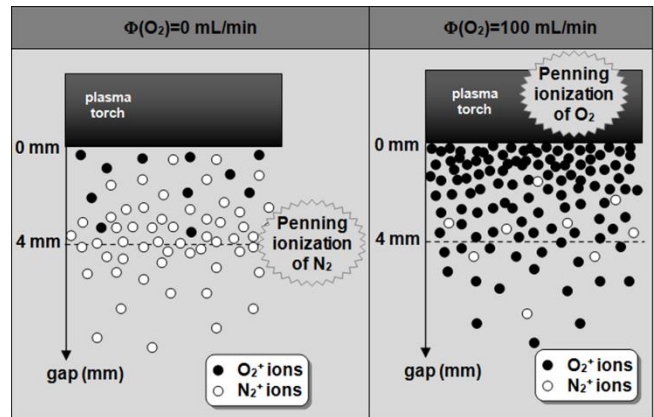


Figure 13. Relation between the mechanisms producing positive ions in the post-discharge and the profile of the DC current measurements.

IV. Conclusion

The flowing post-discharge generated by an RF He- O_2 plasma torch has been characterized by OES, MS and electrical measurements. We have evidenced that the contamination in the flowing post-discharge is similar to the contamination measured in a vacuum chamber at a pressure of 1 Torr. Even if increasing the helium flow rate reduces the atmospheric contamination on several decades, the atmospheric nitrogen and oxygenated species must still be taken into account on the chemical processes in the flowing post-discharge.

By OES, we have identified the excited and positive charged species in the post-discharge and suggested mechanisms

explaining the production of N_2^+ and O_2^+ ions. By electrical characterizations, we have evidenced the existence of a DC current depending mainly on the O_2 flow rate (and in a less extent to the helium flow rate) for small gaps, i.e. lower than 4 mm. The current measured is considered as resulting from a competition between positive and negative charged species. The positive charged species mostly involved in the DC current are the O_2^+ ions. N_2^+ ions are also involved but in a less extent since the Penning ionization of O_2^+ is more efficient than the Penning ionization of N_2^+ . The existence of negatively charged oxygenated species is assumed to play an important role for O_2 flow rates higher than 50 mL/min.

V. Acknowledgments

This work was part of the I.A.P (Interuniversitary Attraction Pole) program financially supported by the Belgian Federal Office for Science Policy (BELSPO). This work was also financially supported by the FNRS (Belgian National Fund for Scientific Research), Région Wallonne (OPTI2MAT Excellence Program) and the European Commission (FEDER – Revêtements Fonctionnels).

VI. References

- [1] U. Kogelschatz, *Plasma Chemistry & Plasma Processing*, **23**, 1, 2003.
- [2] A. Schutze, *Plasma Science, IEEE Transactions on*, 1998, **26**, 6, 1685-1694.
- [3] T. Dufour, R. Dussart, P. Lefauchaux, P. Ranson, L. J. Overzet, M. Mandra, J.-B. Lee, M. Goeckner, *Appl. Phys. Lett.*, **93**, 7, 2008.
- [4] T. Dufour, L. J. Overzet, R. Dussart, L. C. Pitchford, N. Sadeghi, P. Lefauchaux, M. Kulsreshath, P. Ranson, *Eur. Phys. J. D.*, **60**, 3, 565-574, 2010.
- [5] J. Heberlein, A. B. Murphy, *J. Phys. D : Appl. Phys.*, **41**, 2008, 053001, 20 pp.
- [6] P. Freton, J. J. Gonzalez, A. Gleizes, F. Camy Peyret, G. Caillibotte, M. Delzenne, 2002, *J. Phys. D: Appl. Phys.*, **35**, 2, 115-131.
- [7] C. Pardo, J. Gonzalez-Aguilar, A. Rodriguez-Yunta, M. A. G. Calderon, 1999, *J. Phys. D: Appl. Phys.*, **32**, 17, 2181-2189.
- [8] P. Fauchais, *J. Phys. D: Appl. Phys.*, **37**, R86-R108, 2004.
- [9] X. Pei, X. Lu, J. Liu, D. Liu, Y. Yang, K. Ostrikov, P. K. Chu, Y. Pan, *J. Phys. D: Appl. Phys.*, 2012, **45**, 165205.
- [10] Y.-H. Choi, J.-H. Kim, Y. S. Hwang, *Surface & Coatings technology*, 2005, **193**, 319-324.
- [11] M. J. Shenton, G. C. Stevens, *J. Phys. D : Appl. Phys.*, 2001, **34**, 2761-2768.
- [12] Z. Fang, Y. Qiu, Y. Luo, *J. Phys. D : Appl. Phys.*, 2003, **36**, 2980-2985.
- [13] E. Gonzalez II, M. D. Barankin, P. C. Guschl, R. F. Hicks, *Plasma Process. Polym.*, 2010, **7**, 482-493.
- [14] D. Merche, T. Dufour, J. Hubert, C. Poleunis, S. Yunus, A. Delcorte, P. Bertrand, F. Reniers, *Plasma Process. Polym.*, 2012, DOI: 10.1002/ppap.201100208.
- [15] N. Claessens, F. Demoisson, T. Dufour, A. Felten, J. Guillot, J.-J. Pireaux, F. Reniers, *Nanotechnology*, **21**, 38, 2010,
- [16] S. Yonson, S. Coulombe, V. Léveillé, R. L. Leask, *J. Phys. D : Appl. Phys.*, 2006, **39**, 3508-3513.
- [17] K. Landsberg, Ch. Scharf, K. Darm, Th. von Woedtke, *Plasma Medecine*, 2010, **1**, 55-63.
- [18] T. Nosenko, T. Shimizu, G. E. Morfill, *New Journal of Physics*, 2009, **11**, 115013 (19 pp).
- [19] S. P. Kuo, O. Tarasenko, J. Chang, M. Nikolic, *New Journal of Physics*, 2009, **11**, 115016 (17 pp).
- [20] M. G. Kong, G. Kroesen, G. Morfill, J. L. Zimmermann, *New Journal of Physics*, 2009, **11**, 115012 (35 pp).
- [21] J. T. Gudmundsson, *J. Phys. D : Appl. Phys.*, 2004, **37**, 2073.
- [22] J. Y. Jeong, J. Park, R. F. Hicks, *J. Phys. Chem. A*, 2000, **104**, 8027-8032
- [23] R. P. Cardoso, T. Belmonte, G. Henrion, N. Sadeghi, *J. Phys. D: Appl. Phys.*, 2006, **39**, 4178-4185.
- [24] G. C.-Y. Chan, J. T. Shelley, J. S. Wiley, G. M. Hieftje, *Anal. Chem.*, 2011, **83**, 3675-3686.
- [25] Y.-M. Chiu, C.-T. Hung, S.-H. Chen, *Computer Physics Communication*, 2010, 4113.
- [26] J. Goree, B. Liu, D. Drake, *J. Phys. D: Appl. Phys.*, 2006, **39**, 3479-3486.
- [27] Patent US7329608 Surfx Techn., S. E. Babayan, R. F. Hicks, 2008.
- [28] J. Glosik, A. B. Rakshit, N. D. Twiddy, N. G. Adams, D. Smith, *J. Phys. B: Atom. Molec. Phys.*, 1978, **11**, 3365-3379.
- [29] E. Stoffels, Y. A. Gonzalvo, T. D. Whitmore, D. L. Seymour, J. A. Rees, *Plasma Sources Sci. Technol.*, 2006, **15**, 501-506.
- [30] Z. Gavare, D. Gött, A. V. Pipa, J. Röppcke, A. Skudra, *Plasma Sources Sci. Technol.*, 2006, **15**, 391-395.
- [31] Y. Li, Z. Chen, Y.-K. Pu, *Plasma Process. Polym.*, 2005, **2**, 581-585.
- [32] T. Dufour, J. Hubert, P. Viville, C. Duluard, S. Desbief, R. Lazzaroni, F. Reniers, *Plasma Process. Polym.*, 2012, DOI: 10.1002/ppap.201100209.
- [33] J. Y. Jeong, S.E. Babayan, G. S. Selwyn, *Plasma Sources Sci. Technol.*, 1998, **7**, 282-285.
- [34] B. F. Minaev, H. Agren, *J. Chem. Soc., Faraday Trans.*, 1997, **93**, 2231-2239.
- [35] M. Hild, R. Schmidt, *J. Phys. Chem. A*, 1999, **103**, 6091-6096.
- [36] V. Léveillé, S. Coulombe, *Plasma Process. Polym.* 2006, **3**, 587-596.
- [37] K. Kutasi, P. Hartmann, Z. Donko, *J. Phys. D : Appl. Phys.*, 2001, **34**, 3368-3377.
- [38] J. Jolly, M. Touzeau, A. Ricard, *J. Phys. B: At. Mol. Phys.*, 1981, **14**, 473-481.
- [39] M. Cher, C.S. Hollingsworth, *J. Chem. Phys.*, 1969, **50**, 4942.
- [40] G. Taieb, H. P. Broida, *Chemical Physics*, 1977, **21**, 313-316.
- [41] C. B. Collins, Z. Chen, J. Stevefelt, *IEEE Journal of Quantum Electronics*, 1986, **22**, 38-46.
- [42] M. A. Khan, A. M. Al-Jalal, *Journal of Applied Physics*, 2008, **104**, 123302.
- [43] C.E. Moore, P. W. Merrill, Partial Grotrian diagrams of astrophysical interest, National Bureau of standards 23, 1968.
- [44] V. Léveillé, S. Coulombe, *Plasma Sources Sci. Technol.*, 2005, **14**, 467-476.
- [45] S. Popovic, M. Nikolic, J. Upadhyay, L. Vuskovic, 41st Plasmadynamics and Lasers Conference, Chicago, Illinois, June 28-1, 2010.

- [46] J. S. Sousa, K. Niemi, D. O'Connell, *Journal of Applied Physics*, 2011, **109**, 123302.
- [47] C. Lee, D. B. Graves, M. N. Lieberman, D. W. Hess, *J. Electrochem. Soc.*, 1994, **141**, 1546.
- [48] D. Lee, J. Park, S. H. Hong, Y. Kim, *IEEE Trans. Plasma Sci.*, 2005, **33**, 949.
- [49] M. A. Naveed, A. Qayyum, S. Ali, M. Zakauallah, *Physics Letters A*, 2006, 499-503.
- [50] A.A. Ionin, I. V. Kochetov, A. P. Napartovitch, N. N. Yuryshev, *J. Phys. D : Appl. Phys.*, 2007, **40**, 25-61.
- [51] R. K. Datta, K. N. Rao, *Ind. J. Chem. A*, 1979, **18**, 102.
- [52] A. Hicks, S. Norberg, P. Shawcross, W. R. Lempert, J. W. rich, I. V. Adamovich, *J. Phys. D : Appl. Phys.*, 2005, **38**, 3812-3824.
- [53] R. Ono, T. Oda, *J. Phys. D: Appl. Phys.*, 2002, **35**, 2133-2138.
- [54] A. Khacef, J. M. Cormier, J. M. Pouvesle, *J. Phys. D: Appl. Phys.*, 2002, **35**, 1491-1498.
- [55] Y. Itikawa, N. Mason, *J. Phys. Chem. Ref. Data*, 2005, **34**, 1.
- [56] B. Rosen, *Données spectroscopiques relatives aux molécules diatomiques*, Pergamon, Paris, 1970, pp 279-280.
- [57] C.-H. Yi, Y.-H. Lee, D. W. Kim, G.-Y. Yeom, *Surface and Coatings Technology*, 2003, **163-164**, 723-727.